

# Searching for misaligned active galactic nuclei among blazar candidates in the Fourth *Fermi*-LAT catalog.

Graziano Chiaro<sup>a,b</sup>, Giovanni La Mura<sup>c</sup>, Alberto Domínguez<sup>d</sup>, Susanna Bisogni<sup>a</sup>

<sup>a</sup>*Istituto di Fisica Cosmica e Astrofisica Spaziale IASF, INAF Via A. Corti 12, 20133 Milano IT*

<sup>b</sup>*Consorzio Interuniversitario per la Fisica Spaziale CIFS, Via Pietro Giuria, 1, 10125 Torino IT*

<sup>c</sup>*Lab. de Instrumentação e Física Experimental de Partículas LIP, Av. Gama Pinto 2, Lisboa, PT*

<sup>d</sup>*IPARCOS and Department of EMFTEL, Universidad Complutense de Madrid, Av. Séneca, 2, 28040 Madrid, ES*

---

## Abstract

Radio-loud sources with blazar-like properties, but having a jet that does not directly point in the direction of the observer are among the most interesting classes of  $\gamma$ -ray emitters. These sources are known as Misaligned Active Galactic Nuclei (MAGN). Understanding MAGN properties is useful to improve the knowledge of blazar energetics. We searched for new MAGN candidates among the remaining blazars of uncertain type detected by the *Fermi* Large Area Telescope (LAT) using a methodology based on characterizing their radio morphology. We identified seven candidates associated with  $\gamma$ -ray sources. Their features are consistent with a source with a misaligned relativistic jet consistent with the definition of MAGN.

*Keywords:*

---

## 1. Introduction

Launched by NASA on 2008 June 11 the *Fermi* satellite has been observing  $\gamma$ -ray emitters with the Large Area Telescope (LAT) the primary instrument onboard (Atwood et al., 2009). LAT is an imaging, high-energy  $\gamma$ -ray telescope, covering the energy range from below 100 MeV to more than 300 GeV. The Fourth *Fermi*-LAT Source Catalog (4FGL) reports  $\gamma$ -ray data collected by LAT in the first eight years of operation and lists 5065 sources (Abdollahi et al., 2020). Out of these, 3131 sources are blazars, which are divided into 1116 BL Lacertae (BL Lac), 686 Flat Spectrum Radio Quasar (FSRQ) and 1329 blazars candidates of uncertain type (BCU). **These sources are also** reported in the Fourth Catalog of Active Galactic Nuclei (4LAC, Ajello et al., 2020).

Gamma-ray emitters that host an Active Galactic Nucleus (AGN) can be classified according to the orientation of their relativistic jet relative to the line of sight of the observer, as described in the unified model (Urry & Padovani, 1995). In that model, blazars are active galaxies whose jets are seen at a small viewing angle. Another class of AGNs, known as Misaligned Active Galactic Nuclei (MAGN, Abdo et al., 2010b) show a jet of radiation pointed at larger angles to the viewer than blazars. The radio-loud MAGNs are further classified into two main classes according to the distance of the brightest point from the central core (Urry & Padovani, 1995; Abdo et al., 2010b), namely the edge-darkened Fanaroff-Riley I radio galaxies (FR-I) and the edge-brightened Fanaroff-Riley

*Preprint submitted to Elsevier*

*July 30, 2020*

II radio galaxies (FR-II) (Fanaroff & Riley, 1974). Steep Spectrum Radio Quasars (SSRQs), whose jet angles are smaller than those of radio galaxies but larger than those of blazars, are often also considered as MAGNs (Oriente, 2016). We do not include SSRQs in the present analysis. In Saripalli (2012) and in Chiaberge et al. (1999) the authors gave several reasons to support the view that FR-I and FR-II are the parent population of blazars. This interpretation is also supported by the similarity in the radio-to-optical and optical spectral indices of the two classes of sources. From this relationship with blazars, studying MAGNs remains of fundamental importance for the understanding of the AGNs population as a whole, their radiation mechanisms, and their galaxy structure as well as the disparity of detection between more powerful and weaker  $\gamma$ -ray sources (Armeida et al., 2011; Ghisellini et al., 2005; Torresi, 2018). There are 36  $\gamma$ -ray sources classified as MAGN in 4LAC, however the number could be greater if new candidates whose properties are closely related with characteristic MAGN features could be found among the remaining blazars of uncertain type (BCUs). It is the aim of this study to search for such sources.

The paper is organized as follows: Sec. 2 describes our selection criteria and radio data; in Sec. 3 we discuss the results and, finally, Sec. 4 presents a brief conclusion.

## 2. Sample selection and data

In this section, we select potential MAGNs from BCUs in 4LAC based on the  $\gamma$ -ray properties of known MAGNs listed in the catalog. Then, we search for these sources in archival radio data and characterize their extension. This procedure allows us to find the best candidates.

### 2.1. Gamma-ray selection

We began this study by searching for the most probable MAGN candidates from the BCU population in the 4LAC catalog, using the fact that their properties cover only a fraction of the parameter space spanned by blazar spectra. Using a power-law with index  $\Gamma$  to represent the spectra in the form of  $dN/dE \propto E^{-\Gamma}$ , it is found that MAGNs lie within the range  $1.6 < \Gamma < 2.7$ , while blazars generally have  $\Gamma > 1.2$ . Furthermore we considered the Variability Index (VI). This parameter is defined as twice the sum of the log-likelihood difference between the flux fitted in each time interval and the average flux over the full catalog interval and it represents the statistical significance of the variability of a source, with respect to its averaged spectral features. It is a key property of blazars depending on the energy band considered (Ackermann et al., 2003; Abdo et al., 2010c; Hayashida et al., 2012) and explained as emitting electrons in a leptonic scenario of different energies and thus different acceleration/cooling times in the distinct bands. Known MAGNs have  $2.8 < VI < 30$ . This range indicates no significant variability, in contrast to blazars, which are often highly variable, with more of 40% of them having  $VI > 72$  (Ajello et al., 2020). We applied these two criteria to the BCU sources selecting 1062 candidates.

### 2.2. Radio data

A key parameter for a rigorous misaligned AGN classification is the orientation angle of the relativistic jet relative to the line of sight. Yet this parameter is difficult to determine through observations and most of the methods in the literature provide uncertain

measurements or limits (Landt et al., 2002; Giovannini et al., 1994). Approximate estimates of the inclination can be obtained from measurements of the projected size of the extended emission, if we can make assumptions on the intrinsic size of the sources. Unfortunately, the observed differences in the extension of powerful radio galaxies seen at very large angles only allow to place weak constraints on the limiting values of the inclination angle. Furthermore, it is not obvious what angle defines the frontier between a blazar and a MAGN. Another method to measure the orientation angle of an AGN jet relies on the determination of the [O III]  $\lambda 5007$  emission line equivalent width. Since the line radiation is emitted almost isotropically from an extended ionized region, while the underlying AGN continuum is prone to obscuration, most likely close to the plane of the accretion disk, the ratio of the corresponding intensities is expected to depend on the inclination of the source (Risaliti et al., 2011; Bisogni et al., 2017, 2019). In this case, the main factors of indetermination are the uncertainty in the relation between the AGN continuum and the emission line, which depends on the covering factor and the distribution of the ionized gas, and the possible differences among the jet orientation and the distribution of the obscuring material. However, searching for the sources in our sample in the spectroscopic databases of the Sloan Digital Sky Survey (SDSS, York et al., 2000; Aguado et al., 2019), of the 6dF Galaxy Redshift Survey (6dFGS, Jones et al., 2004, 2009), as well as in dedicated spectroscopic campaigns of 4FGL BCU lists (de Menezes et al., 2020), only 7 spectra could be found. These were BL Lac or elliptical galaxy spectra, with no indications of emission line features. By definition, these objects are not suitable for the [O III]  $\lambda 5007$  equivalent width method. Therefore, we looked for other alternatives based on radio data. We searched for radio counterparts in the NRAO VLA Sky Survey (NVSS)<sup>1</sup>, in the Sydney University Molonglo Sky Survey (SUMSS)<sup>2</sup>, and in the Faint Images of the Radio Sky at Twenty-cm (FIRST)<sup>3</sup>. Since a MAGN defining feature is the observation of a radiative jet not pointing close to the line of sight, MAGNs will appear as sources with an extended morphology, as opposed to the compact core-dominated shape of blazars. Unfortunately, the angular resolution of the surveys that cover the largest portions of sky, namely NVSS and SUMSS, is of the order of 30 arcsec or worse, and it is not suitable to assess the actual morphology of the selected targets. However, by comparing the NVSS images of objects that were also observed at the resolution of 5 arcsec in the FIRST survey, we are able to verify that the presence of extended structures in the high resolution observations reflects into asymmetric or elongated shapes in the low resolution images. Indeed, angular sizes significantly larger than the survey beam size can actually correspond to objects with a confidently detectable extended radio component. By selecting objects with a major axis larger than 45 arcsec from the NVSS and objects with a corresponding axis larger than 70 arcsec from the SUMSS, to account for its lower image quality, we are able to find sources with the strongest evidence of an extended radio emission component. We restricted the list of candidates only to sources with a strong indication of extended contributions in both data sets considering the ratio (MajAxis) / (MinAxis) > 1.5 consistent with an extended structure. According to the previous criteria, first, relative to the NVSS/FIRST selection and second, relative to the SUMSS selection, there are 25 and 23  $\gamma$ -ray sources, respectively. These 48 candidates represent the master sample of our study and are listed in Table 1. We subsequently inspected the radio images of these candidates, in order to separate those with a confident extended structure from objects where the radio morphology was affected by noisy patterns or by the overlapped contribution of nearby sources. In this way, we obtained another list of seven objects with evidence of extended emission, collected in Table 2, five of which have publicly available optical spectra.

---

<sup>1</sup><http://www.cv.nrao.edu/nvss/>

<sup>2</sup><http://www.astrop.physics.usyd.edu.au/sumsscat/>

<sup>3</sup><http://sundog.stsci.edu/>

Table 1: The master sample. The table columns represent, respectively, the 4FGL source name, the name of the low-energy counterpart associated in 4FGL, the radio coordinates and the angular size of the major axis expressed in arcmin, as measured by the relevant radio survey.

Source Name	assoc 4FGL	RA radio	DEC radio	MajAxis
4FGL J0011.8-3142	SUMSS J001141-314220	2.923	-31.705	1.42
4FGL J0015.9+2440	GB6 J0016+2440	4.015	24.670	2.7
4FGL J0119.6+4158	2MASX J01200274+4200139	20.008	42.002	0.91
4FGL J0119.9+4053	CRATES J012018+405314	19.949	40.905	1.42
4FGL J0143.5-3156	PKS 0140-322	25.966	-31.901	0.50
4FGL J0201.1-4347	GALEXASC J020110.83-434654.8	30.294	-43.781	1.19
4FGL J0228.2-3102	PMN J0228-3102	37.054	-31.044	1.42
4FGL J0233.5+0654	2MASS J02334098+0656114	38.377	6.923	0.76
4FGL J0240.8-3401	NVSS J024047-340018	40.198	-34.005	1.28
4FGL J0301.4-3124	AT20G J030116-312615	45.318	-31.438	1.29
4FGL J0325.3+3332	2MASX J03251760+3332435	51.323	33.545	2.11
4FGL J0338.9-2848	NVSS J033859-284619	54.747	-28.799	2.28
4FGL J0342.8-3007	PKS 0340-302	55.667	-30.132	1.42
4FGL J0345.5-3301	2MASS J03453818-3256462	56.373	-32.934	1.42
4FGL J0348.8+4610	B3 0345+460	57.327	46.166	0.93
4FGL J0507.9+4647	TXS 0503+466	76.848	46.761	1.34
4FGL J0536.0-2754	PMN J0535-2751	83.965	-27.865	1.02
4FGL J0551.8-3517	NVSS J055142-351527	88.027	-35.296	1.35
4FGL J0602.7-0007	PMN J0602-0004	90.679	-0.074	1.13
4FGL J0632.0-1032	TXS 0629-105	97.969	-10.564	1.33
4FGL J0637.4-3537	WISE J063746.40-353648.3	99.440	-35.615	1.28
4FGL J0828.6-0747	NVSS J082854-074854	127.227	-7.815	1.08
4FGL J0829.7-5856	PMN J0829-5856	127.476	-58.959	1.20
4FGL J0928.2-3048	PKS 0926-306	142.141	-30.828	1.42
4FGL J0929.3-2414	NVSS J092928-241632	142.366	-24.275	1.3
4FGL J1008.8-3139	PKS 1006-313	152.210	-31.651	1.42
4FGL J1111.8+4858	1RXS J111157.8+485725	167.991	48.948	1.01
4FGL J1208.4+6121	RGB J1208+613	182.156	61.355	1.44
4FGL J1215.8-3732	PMN J1215-3734	184.008	-37.570	1.28
4FGL J1223.6-3032	NVSS J122337-303246	185.905	-30.546	0.96
4FGL J1232.5-3720	NVSS J123235-372051	188.149	-37.347	1.28
4FGL J1344.4-3656	PKS 1341-366	206.098	-36.941	1.28
4FGL J1455.4-3654	PKS 1452-367	223.787	-36.925	1.48
4FGL J1457.8-4642	PMN J1457-4642	224.426	-46.701	2.22
4FGL J1507.3-3710	NVSS J150720-370903	226.838	-37.205	1.28
4FGL J1523.2-3941	2MASS J15234352-3936318	230.887	-39.611	1.07
4FGL J1530.5-3026	NVSS J153041-302559	232.671	-30.432	1.42
4FGL J1549.8-3044	NVSS J154946-304501	237.444	-30.750	1.44
4FGL J1628.3-3343	NVSS J162819-334342	247.082	-33.728	1.42
4FGL J1643.7+3317	NVSS J164339+331640	250.916	33.277	1.22
4FGL J1741.9+2555	NVSS J174147+255443	265.473	25.949	0.90
4FGL J1742.4-1518	PMN J1742-1517	265.548	-15.291	2.10
4FGL J2002.6+6302	1RXS J200245.4+630226	300.687	63.041	0.99
4FGL J2046.6-1012	PMN J2046-1010	311.727	-10.178	1.58
4FGL J2049.0+1647	NVSS J204902+164727	312.260	16.790	0.95
4FGL J2229.1+2254	NVSS J222913+225511	337.307	22.919	0.75
4FGL J2309.7-3632	1RXS J230940.6-363241	347.418	-36.541	1.29

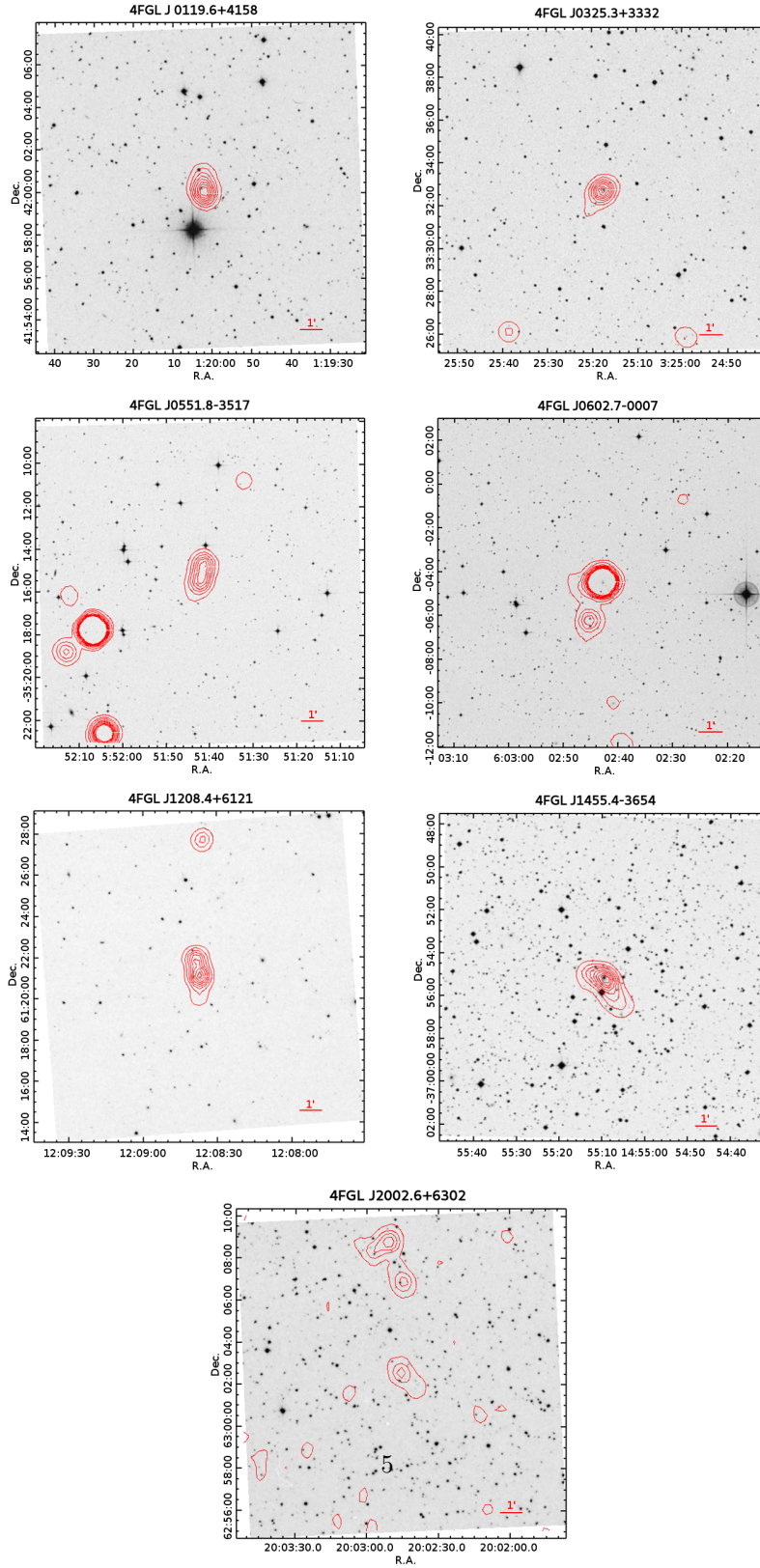


Figure 1: Optical images and NVSS radio contour maps of the best MAGN candidates of the sample (see Table 2). In spite of the low survey observations resolution, all the candidates show an asymmetric extended component.

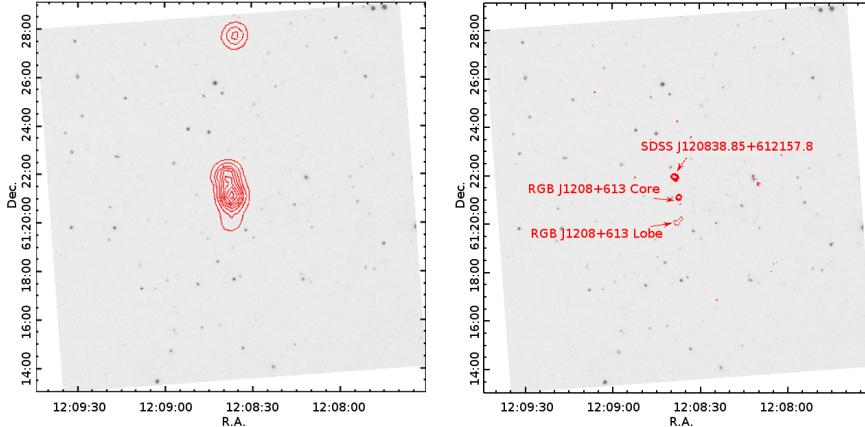


Figure 2: Comparison of the low resolution NVSS radio contour map of RGB J1208+613 (left panel) with the high resolution FIRST observation of the same source (right panel).

### 3. Results

#### 3.1. Properties of our MAGN candidates

The sources that have been identified in this study are all radio emitters with a clear detection in major all-sky radio surveys. The radio spectra tend to be rather flat or with indications of significant emission at high frequency, as inferred from the inclusion of these targets in lists of objects with flat radio spectra, such as the CLASS radio survey and the CRATES catalogue (Myers et al., 2001; Healey et al., 2007), or by their detection with high frequency observations, like the AT20G survey at 20 GHz (Murphy et al., 2010; Massardi et al., 2010).

Table 2 presents the best MAGN candidates found in this study, presenting measurements of their angular size, together with additional information about their detection at X-ray frequencies, the availability of redshift and spectroscopic information and the corresponding projected sizes. Figure 1 shows radio contours plotted on top of optical images. These sources have radio images that show hints of partially resolved asymmetric structures, which point to the existence of an extended component. This interpretation can only be confirmed through the analysis of higher resolution radio images. The only case for which this test is possible, among our seven candidates, comes from the comparison of the low-resolution NVSS image and the high-resolution FIRST observation of RGB J1208+613 (4FGL J1208.4+6121), a galaxy located at  $z = 0.275$ . This comparison, illustrated in Figure 2, reveals that the extended structure is produced by the presence of two bright hot spots, symmetrically distributed around the source. While the northern feature is probably associated with the emission of a nearby quasar, SDSS J120838.85+612157.8 located at  $z = 0.525$ , the southern one appears as the termination of an extended emission, without other counterparts, that likely originated from RGB J1208+613 itself.

Although at the low resolution of the available survey images we are not able to infer the intrinsic structure of the radio sources, all the selected candidates feature an extended component. The emission is still core-dominated, but, unlike the case of blazars, which tend to be compact and symmetric, these objects show an extended structure that suggests hints of partially resolved morphology. These are more often asymmetric and one-sided, although in a smaller number of cases we can observe hints of two-sided emission. The core of the radio source is typically associated with a visible optical counter-part, which has faint or no detectable X-ray emission.

Table 2: Properties of the best MAGN candidates. The table reports a measurement of the angular size of the extended emission, the redshift (if available), the corresponding scale, the projected size, a flag stating whether the source is detected in X-rays and the origin of the optical spectrum.

Source Name	Ang. Size arcmin	$z$	Scale $\text{kpc} \cdot \text{arcsec}^{-1}$	Proj. Size kpc	X-ray det.	Spec. Ref. <sup>a</sup>
4FGL J0119.6+4158	$1.41 \pm 0.20$	0.109	2.003	$169.4 \pm 24.0$	no	deM
4FGL J0325.3+3332	$1.46 \pm 0.20$	0.128	2.303	$201.7 \pm 20.7$	no	deM
4FGL J0551.8-3517	$1.50 \pm 0.15$	–	–	–	yes	–
4FGL J0602.7-0007	$1.14 \pm 0.25$	0.118	2.147	$146.8 \pm 32.2$	yes	deM
4FGL J1208.4+6121	$1.37 \pm 0.15$	0.274	4.215	$346.5 \pm 37.9$	yes	SDSS
4FGL J1455.4-3654	$1.81 \pm 0.30$	0.095	1.774	$192.6 \pm 31.9$	yes	6dF
4FGL J2002.6+6302	$1.41 \pm 0.25$	–	–	–	yes	–

<sup>a</sup> deM = de Menezes et al. (2020)

SDSS = Sloan Digital Sky Survey

6dF = 6 degree Field Galaxy Redshift Survey

Exceptions to the association of the radio sources with optical counterparts are generally occurring in objects that lie close to the Galactic plane, for which an effect of severe absorption prevents the observation of the visible light. The lack of a strong X-ray emission and the more abundant detection of asymmetric radio structures, over symmetric ones, are all indications of an intermediate inclination of the jets produced by these sources between the blazar and the radio galaxy regime. The spectra of the optical sources, when available, are also consistent with spectra of elliptical galaxies, characterized by strong absorption lines (Jones et al., 2004, 2009; York et al., 2000; Aguado et al., 2019; de Menezes et al., 2020). These characteristics pose the sources belonging to our sample at an intermediate stage between closely aligned blazars and AGN with jets pointing at large angles relative to us, in agreement with our identification as new  $\gamma$ -ray MAGNs.

### 3.2. TeV candidates

We also checked the detectability at the TeV energy range for the MAGN candidates highlighted in Table 2. For this purpose we reviewed the  $\gamma$ -ray spectra of these sources, which are shown in Figure 3.2. We note that all of these sources are faint, with integrated energy fluxes from 100 MeV to 100 GeV lower than  $8 \times 10^{-12}$  erg/cm<sup>2</sup>/s, and none of them has been detected by LAT at energies larger than about 30 GeV, except J2020.6+6302. For confirming this, we searched for these sources in the Third Catalog of Hard *Fermi*-LAT sources (3FHL, Ajello et al. 2017) and in the Second Catalog of Hard *Fermi*-LAT sources (2FHL, Ackermann et al. 2016). The former describes sources detected above 10 GeV in the first 7 years of mission, whereas the latter describes sources detected above 50 GeV in the first 6.7 years of mission. None of these sources are in 2FHL, and only two, J1208.4+6121 and J2002.6+6302, are in 3FHL. However, they are too faint to be detectable with Imaging Atmospheric Cherenkov Telescope (IACTs) in reasonable exposures unless they undergo a flare.

## 4. Summary and conclusions

We expanded the known population of 36 MAGNs currently classified in the 4LAC catalog by finding seven new candidates in the BCU population. Our method based on the morphological characterization of radio archive images and the study of the available optical observations identifies objects with strong evidence of MAGN nature, though only better resolution images can give conclusive evidence. Due to their radiative weakness, these sources cannot be observed in the TeV energy range.

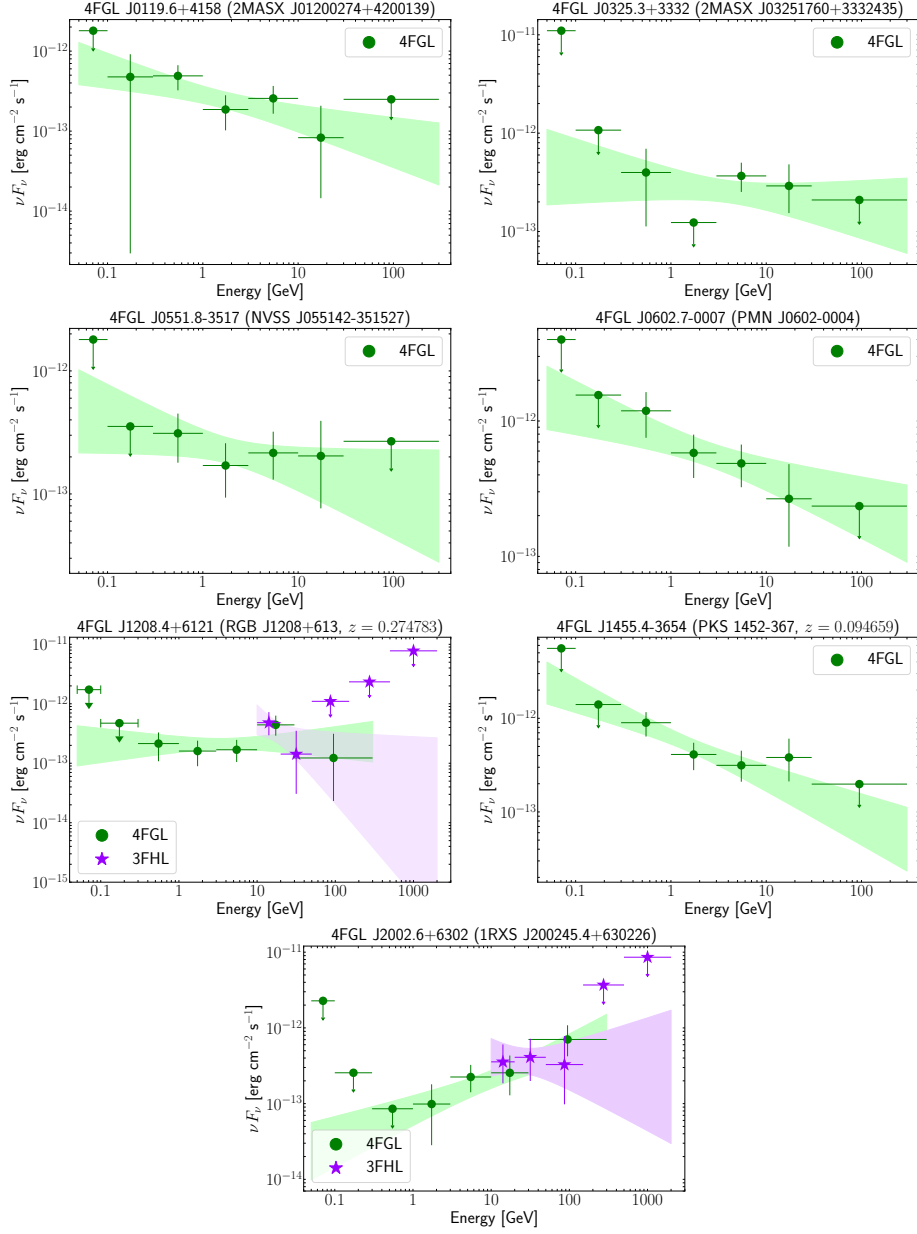


Figure 3: Spectral data of our seven MAGN candidates from 4FGL (green) and 3FHL (violet). Note that the two catalogs are built using different exposures, therefore there may be variability issues between them. This figure shows that sources are faint and they can hardly be detected by IACTs.

## 5. Acknowledgments

Support for science analysis during the operation phase is gratefully acknowledged from the *Fermi*-LAT Collaboration for making the *Fermi*-LAT results available in such a useful form, the Institute of Space Astrophysics and Cosmic Physics in Milano - Italy (IASF), National Institute for Astrophysics (INAF) Rome - Italy and the Lab. de Instrumentacao e Fisica Experimental de Particulas. LIP, Lisboa, PT. A.D. acknowledges the support of the Ramón y Cajal program from the Spanish MINECO. The authors would like the anonymous referee for discussion and suggestions leading to the improvement of this work.

## 6. Bibliography

### References

- Abdo A.A. et al., 2010a, ApJ, 716,1  
Abdo A.A. et al., 2010b, ApJ, 720, 912  
Abdo A.A. et al., 2010c, Nature, 463, 919  
Abdollahi S. et al., 2020, ApJS 247, 33  
Ackermann M. et al, 2003, ApJ, 771, 57  
Ackermann M. et al., 2012, ApJ, 753, 83  
Aguado D. S. et al., 2019, ApJS, 240, 23  
Ajello M. et al., 2017, ApJS,232,18  
Ajello M. et al., 2020, ApJ, 892, 105  
Armeida C.R. et al., 2011 MNRAS, 410,3  
Atwood W.B. et al., 2009, ApJ, 697, 1071  
Bisogni S. et al., 2017, MNRAS, 464, 385B  
Bisogni S. et al., 2019, MNRAS, 485, 1405B  
Chiaberge A. et al., 1999, MNRAS,349,77  
de Menezes R. et al., 2020, Ap&SS, 365, 12  
Fanaroff B. L., Riley J. M., 1974, MNRAS, 167, 31  
Giovannini G. et al, 1994, ApJ, 435,116.  
Ghisellini G. et al., 2005; AA 432,401  
Ghisellini G., 2013, EPJ Web of Conference, Vol. 61, id.05001  
Hayashida K. et al., 2012, ApJ, 754, 114  
Healey S. E. et al., 2007, ApJS, 171, 61  
Jones D. et al., 2004, MNRAS 355, 747  
Jones D. et al., 2009, MNRAS, 399, 683  
Landt H. et al., 2002, MNRAS, 336,945.  
Massardi M. et al., 2011, MNRAS, 412, 318  
Migliori G. et al., 2011 A&A 72, 593  
Murphy T. et al., 2010, MNRAS, 402, 2403  
Myers S. T. and the CLASS Collaboration, ASPC, 237, 51  
Orienti M., 2016, AN, 337, 2  
Risaliti G. et al., 2011, MNRAS, 411, 2223R  
Saripalli L., 2012, AJ, 144,85  
Torresi E., 2018, arXiv 1809.08074  
Urry M.C., Padovani P., 1995, ASP, 107, 803  
York D.G. et al., 2000, AJ, 120, 1579